Fluid simulation of a pulsed-power inductively coupled argon plasma

D. P. Lymberopoulos
Applied Materials, 3100 Bowers Avenue, Santa Clara, California 95054

V. I. Kolobov[a] and D. J. Economou
Plasma Processing Laboratory, Department of Chemical Engineering, University of Houston, Houston, Texas 77204-4792

(Received 12 June 1997; accepted 31 October 1997)

A one-dimensional fluid model was developed and used to investigate the spatiotemporal dynamics of a pulsed-power inductively coupled argon plasma at 10 mTorr. Particular attention was devoted to extraction and acceleration of positive ions by a radio frequency (rf) bias applied in the afterglow stage of the discharge. For bias frequencies in the range $\omega/2\pi = 100$ kHz–10 MHz the rf sheath is resistive in nature. Significant oscillations of the ion flux at the driven electrode observed at $\omega\tau \approx 1$ are related to the finite ion transit time τ through the sheath. The latter depends on the sheath thickness which is a complicated function of time in the pulsed plasma. For a constant time-average power, the time-average ion energy flux bombarding the wafer has a minimum with respect to the pulse period. This has implications for the wafer thermal budget. © *1998 American Vacuum Society*. [S0734-2101(98)00302-9]

I. INTRODUCTION

Low pressure high density plasmas are widely used in advanced semiconductor manufacturing for fabrication of submicron features. Pulsed plasmas (in which the power is turned on and off with a predetermined period and duty cycle) have been shown to offer important advantages including (a) improved etch selectivity by modifying the ratio of chemical species present in the plasma;[1,2] (b) improved etch or deposition rate (for the same time-average power) compared to continuous wave (cw) discharges,[3–5] (c) reduced dust generation in the plasma,[6,7] and (d) improved etch or deposition uniformity.[2,5,8]

Recently, it has been recognized[9–11] that pulsed plasma operation can ameliorate anomalous etch profiles (e.g., notching) and other undesirable effects that occur in conventional cw discharges. Due to the large difference in electron and ion temperatures in a cw discharge, positive ions bombarding the wafer have a strongly anisotropic velocity distribution, while that of electrons is almost isotropic. As a result positive ions can penetrate deeply into a trench charging the trench bottom positively, while electrons deposit their charge on the sidewalls of the trench.[12–14] Such charging, and the associated etch profile distortions, have become a major problem for the fabrication of the next generation of microdevices.

The situation becomes more favorable in pulsed-power discharges. Recent studies indicate that extraction of charged species from the afterglow plasma and their acceleration towards a radio frequency (rf) biased electrode could dramatically reduce charging damage and improve etching characteristics.[10,15] For instance, greatly improved etch performance has been reported in pulsed-power chlorine discharges by applying a low frequency (<600 kHz) bias to the substrate in the afterglow of an inductively coupled plasma (ICP) source.[10] It was suggested that low frequency bias results in alternate acceleration of positive and negative ions extracted out of the plasma. Since positive and negative ions have almost equal masses and similar velocity anisotropy under the influence of rf bias, the net charge deposited on the wafer surface is almost zero, preventing charge induced damage.

The properties of pulsed-power high density plasmas have not been thoroughly studied so far. Zero-dimensional or ''global'' models have been reported for analyzing the discharge behavior.[16,17] A two-dimensional fluid model was used in Ref. 18 for ICP modeling without separate rf bias. No spatial distributions of plasma parameters were reported in that work. A one-dimensional fluid model of pulsed capacitively coupled discharges in electronegative gases was developed in Ref. 19. Decaying afterglow plasmas in pulsed dc discharges have been investigated in some detail,[20] including kinetic treatment of electrons. It was found that in low pressure (100s of mTorr) collisional plasmas of rare gases, the electron density and temperature decay mainly due to the escape of hot electrons to the walls (diffusion cooling) rather than due to electron energy loss in collisions with gas species. The afterglow of collisional (50–500 mTorr) pulsed dc discharges in oxygen was studied in Ref. 21. High density plasmas used for etching operate at even lower gas pressures, in the near-collisionless regime. No analysis of the spatiotemporal plasma dynamics under these conditions has been reported yet.

The presence of a rf bias can modify the plasma potential and charged particle fluxes towards the walls. The properties of the rf sheath formed in the vicinity of a biased substrate depend on the degree of ion response to the applied excitation frequency. In low density capacitively coupled discharges, the sheath is typically capacitive in nature for frequencies above several MHz, i.e., the displacement current in the sheath typically exceeds the conduction current. In high density plasmas, however, the sheath may be resistive in nature even for frequencies exceeding 10 s of MHz. The prod-

[a]Current address: CFD Research Corporation, 215 Wynn Drive, Huntsville, AL 35805.

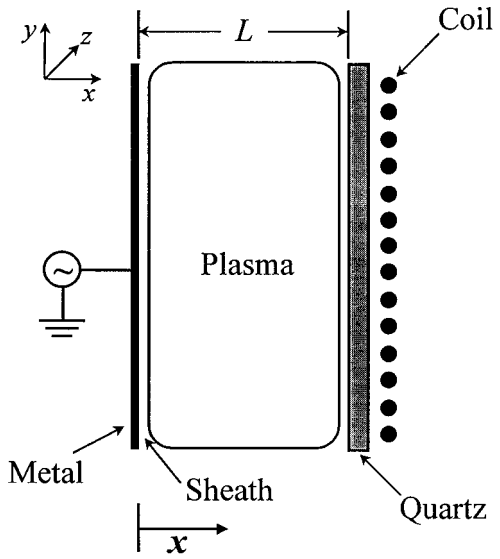

FIG. 1. Schematic of a one-dimensional model discharge. The antenna coil is powered by a current source that can be square-wave modulated with different pulse periods. The left electrode can be biased or grounded.

uct $\omega\tau$ of driving frequency ω and ion transit time through the sheath τ is a fundamental parameter that governs the sheath properties.[22–24] In the limit $\omega\tau \ll 1$, ions respond to the instantaneous sheath field; in the opposite extreme, $\omega\tau \gg 1$, ions respond to the time-averaged sheath field. In the intermediate cases, $\omega\tau \approx 1$, the sheath dynamics may become rather complicated. In high density plasmas, for typical bias frequencies $\omega\tau < 1$ and the sheath is resistive in nature.[22] A self-consistent simulation of the rf sheath dynamics in high density pulsed-power plasmas has not been reported yet.

This article reports results of a self-consistent one-dimensional fluid simulation of a pulsed-power ICP argon plasma. Emphasis is placed upon the decaying plasma at the power-off phase of the cycle, especially the influence of a rf bias on the dynamics of the rf sheath, and ion flux to the driven electrode. Section II describes the discharge model, Sec. III presents the simulation results, and Sec. IV contains the summary and conclusions.

II. DISCHARGE MODEL

A schematic of the model discharge is shown in Fig. 1. The discharge was assumed to be infinite in the y and z directions with all parameters varying only in the x direction. This assumption allows the study of the essential plasma physics without using large computational resources required for solution of multidimensional problems. Plasma species were treated as three separate fluids (electrons, ions, and neutrals) interacting with each other due to collisions. The basic equations are as described in Golant,[25] and have been presented before.[26]

A. Basic equations

The continuity equation for plasma species k is

$$\frac{\partial n_k}{\partial t} = -\frac{\partial \Gamma_k}{\partial x} + \sum_j R_{kj}, \tag{1}$$

where n_k is the density of species k (electrons, positive ions Ar^+, or metastables Ar*), Γ_k is the x component of their flux, and the sum contains all reactions that produce or consume these species each with a rate R_{kj}. Collisional processes included in our model of argon discharge are shown in Table I.[27]

We used an approximate momentum equation for electrons [Eq. (2)] assuming that electron inertia can be neglected. Thus, the electron flux, $\Gamma_e = n_e u_e$, was obtained as the superposition of diffusion and drift under the influence of the electrostatic field $E_x = -\partial V/\partial x$

$$\Gamma_e = -D_e \frac{\partial n_e}{\partial t} - n_e \mu_e E_x, \tag{2}$$

where D_e is the electron diffusion coefficient and μ_e is the electron mobility. The rf heating field does not appear in Eq. (2) because the rf field has only a y component (see below). In addition, the ponderomotive force[28] was neglected.

The full momentum equation was used for ions

$$\frac{\partial}{\partial t}(n_i u_i) + \frac{\partial}{\partial x}(n_i u_i u_i) = -\frac{q n_i}{M}\frac{\partial V}{\partial x} - \frac{kT_i}{M}\frac{\partial n_i}{\partial x} - n_i u_i \nu_{ia}, \tag{3}$$

where M is the Ar^+ ion mass, k is the Boltzmann constant, T_i is the ion temperature (assumed constant), q is the unit charge, and ν_{ia} is an effective ion collision frequency with neutral atoms.

An energy equation for the ions or neutrals was not solved. Typical values were assumed for the ion temperature ($kT_i/q = 0.11$ eV) and the neutral gas temperature (T_g

TABLE I. Important collisional processes in the argon discharge. Rate coefficients for processes 1–4 are given as a function of electron energy in Fig. 2 of Ref. 27. Units are cm^{+3}/s except for k_{3q} which is in cm^6/s.

No.	Process	Reaction	H_j (eV)	Rate coefficient
1	Ground state excitation	$Ar + e \rightarrow Ar^* + e$	11.56	k_{ex}
2	Ground state ionization	$Ar + e \rightarrow Ar^+ + 2e$	15.7	k_i
3	Stepwise ionization	$Ar^* + e \rightarrow Ar^+ + 2e$	4.14	k_{si}
4	Superelstatic collisions	$Ar^* + e \rightarrow Ar + e$	−11.56	k_{sc}
5	Quenching to resonant	$Ar^* + e \rightarrow Ar^r + e$		$k_r = 2\times10^{-7}$
6	Metastable pooling	$Ar^* + Ar^* \rightarrow Ar^+ + Ar + e$		$k_{mp} = 6.2\times10^{-10}$
7	Two-body quenching	$Ar^* + Ar \rightarrow 2Ar$		$k_{2q} = 3\times10^{-15}$
8	Three-body quenching	$Ar^* + 2Ar \rightarrow 3Ar$		$k_{3q} = 1.1\times10^{-31}$

$=500$ K). Assuming a Maxwellian electron energy distribution function (EEDF), the electron temperature T_e was found from the energy balance equation

$$\frac{\partial}{\partial t}\left(\frac{3}{2}\, n_e k T_e\right) = -\frac{\partial q_e}{\partial x} + W - \tfrac{3}{2}\nu_m \delta n_e k (T_e - T_g) - \sum_i R_i H_i, \tag{4}$$

where W is the power absorbed by electrons from the rf electric field [see Eq. (9)], H_i is the electron energy lost in an inelastic collision of i kind, $\delta = 2m/M$ is the fraction of electron energy lost in elastic collisions with heavy particles, m is the electron mass, and ν_m is the electron elastic collision frequency. The electron energy flux q_e is composed of heat conduction and convection

$$q_e = -K_e \frac{\partial T_e}{\partial x} + \frac{5}{2}\, k T_e \Gamma_e, \tag{5}$$

where K_e is the electron thermal conductivity. Owing to the high thermal conductivity, the electron temperature is almost spatially uniform; its value is governed by the spatially averaged energy gain and loss.

The spatial distribution of power deposition is governed by the space-time variation of the inductive electric field E_y and the rf current density j_y flowing in the plasma. For a harmonic variation of the coil current with a frequency ω_0, the amplitude of E_y satisfies the complex equation

$$\frac{d^2 E_y}{dx^2} + \omega_0 \mu \epsilon E_y = -\mu J_y, \tag{6}$$

where μ is the permeability, ϵ is the permittivity of the medium, and J_y is the total current density (in the coil, plasma, and metallic walls). The relation between the rf current density in the plasma j_y and the rf electric field E_y may be nonlocal, giving rise to the anomalous skin effect[29] and ''collisionless'' electron heating.[30–32] In the present work we used the cold plasma approximation $j_y = \sigma E_y$ with the complex plasma conductivity

$$\sigma = \frac{n_e q^2}{m(\nu_{\text{eff}} + i\omega_0)}, \tag{7}$$

where ν_{eff} is the effective collision frequency, which is a function of the electron speed. The dielectric constant of plasma is obtained from

$$\epsilon_p = \epsilon_0 - \frac{i\sigma}{\omega_0}. \tag{8}$$

Equation (6) was solved in the whole domain including the coil, dielectric window, and plasma. The boundary condition $E_y = 0$ was imposed at $x = 0$. Knowing the heating field, the power absorption by the plasma electrons was found as

$$W = \tfrac{1}{2} R_e(\sigma E_y^2). \tag{9}$$

Finally, the electrostatic potential was found by solving Poisson's equation

$$\frac{d^2 V}{dx^2} = \frac{-q}{\epsilon_0}(n_i - n_e), \tag{10}$$

where ϵ_0 is the permittivity of vacuum. Equation (10) provides the electrostatic field that accelerates charged particles in a direction normal to the electrodes, while Eq. (6) provides the electromagnetic field that heats up the plasma. Capacitive coupling from the coils was assumed to be blocked by a Faraday shield.

B. Boundary conditions

The electron flux at the boundaries was set equal to the thermal flux

$$\Gamma_e = n_e u_T / 4, \tag{11}$$

where $u_T = (8kT_e/\pi m_e)^{1/2}$ is the mean electron velocity. The electron energy flux is given by

$$q_e = \tfrac{5}{2} k T_e \Gamma_e. \tag{12}$$

For the ion density and velocity the second derivative was set equal to zero. The flux of argon metastables to the walls was set equal to the thermal flux, using an equation similar to Eq. (11).

The potential of the left electrode ($x = 0$) was set according to

$$V = V_{\text{dc}} + V_{\text{rf}} \sin(\omega t), \tag{13}$$

where ω is the bias frequency, and V_{dc} was set equal to zero for the results reported herein. The bias was applied in the power-off stage of the discharge, over a certain period of time. The boundary at $z = L$ was either a grounded surface with $V(L,t) = 0$ or a dielectric surface with potential $V(L,t)$ found from the current balance equation

$$j_i - j_e + \epsilon_0 \frac{\partial E}{\partial t} = \frac{\epsilon_i}{d_i}\frac{\partial V}{\partial t}. \tag{14}$$

Here ϵ_i and d_i are the permittivity and thickness of the dielectric wall, respectively. The coupled system of the partial differential equations shown above with the associated boundary conditions was discretized in space using the Galerkin finite element method.[33] The resulting set of differential/algebraic equations was solved simultaneously by a variable order, variable time step integrator, LSODI.[34] It is important to note that the sheath is resolved in the present simulation by having a dense finite element grid near the walls. The computational burden is bearable in this one-dimensional case. However, a separation of the bulk plasma from the sheath is advisable in multidimensional simulations.[35]

III. SIMULATION RESULTS

The first part of this section describes the discharge dynamics without rf bias. The second part examines the influence of rf bias pulse applied in the afterglow stage of the discharge.

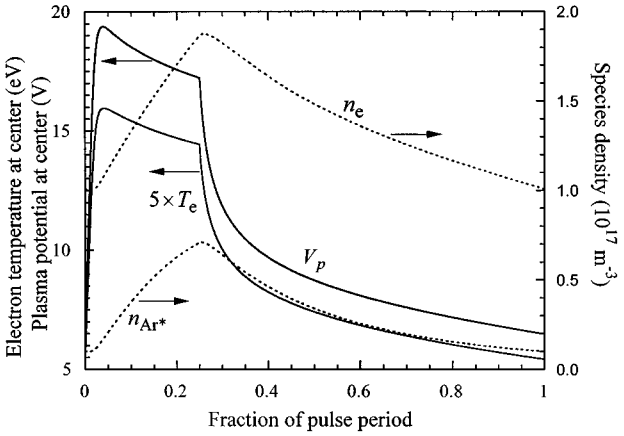

FIG. 2. Time evolution of the electron (ion) density, electron temperature, plasma potential, and metastable atom density at the discharge center for a pulse period of 100 μs. No electrode bias.

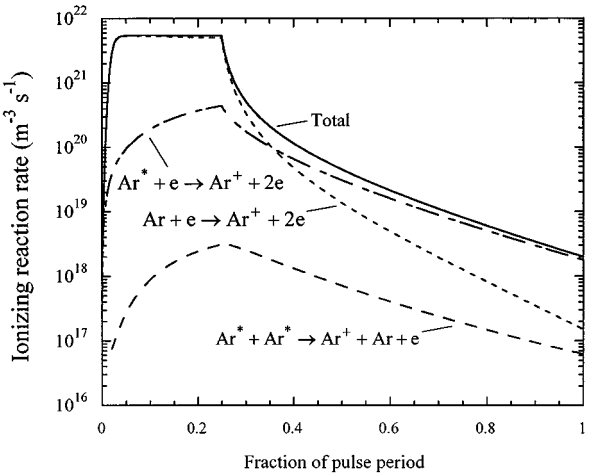

FIG. 3. Time evolution of the rate of various ionization channels at the discharge center for a pulse period of 100 μs. No electrode bias.

A. Spatio-temporal plasma dynamics without rf bias

Simulations were performed for an argon pressure of 10 mTorr, and a gap length of 15 cm. The antenna coil was assumed to be driven by a current source at $\omega_0/2\pi = 2$ MHz. The coil current was square-wave modulated with a period T_p varying between 10 and 500 μs (base case was 100 μs) and a duty cycle of 25%. The current was adjusted to obtain the defined power deposition. The time axis of all figures shown below was normalized to the pulse period T_p. Thus, the power was ON for dimensionless times between 0 and 0.25 and OFF for dimensionless times between 0.25 and 1.0. Results shown herein are for a discharge allowed to relax to the periodic steady state; this would normally occur after a few pulse periods.

The time evolution of important plasma parameters at the discharge center is shown in Fig. 2, for a pulse period of 100 μs. Plasma density, electron temperature, plasma potential, and metastable density all decrease during the power-off fraction of the cycle (0.25–1.0). The time scale of electron (and ion) density decay is that of ion loss to the walls. The time scale of electron temperature decay is that of electron energy loss to the walls which is dominated by the escape of fast electrons in the tail of the distribution. The plasma potential follows the electron temperature, while the metastable density decays by electron impact deexcitation, diffusion to the walls, and metastable–metastable (pooling) reactions (see Table I). Two-body and three-body quenching are negligible under these conditions.

The temporal evolution of the rate of various ionization channels at the discharge center is shown in Fig. 3. It is seen that direct ionization, which is the dominant source of ionization in the active discharge, drops rapidly in the power-off fraction of the period due to decreasing electron temperature. Stepwise ionization becomes the main source of electron generation in the afterglow after dimensionless time 0.35. Ionization by metastable pooling reactions is relatively unimportant in this case of 100 μs pulse period. However, for a pulse period of 500 μs, it becomes comparable to stepwise ionization in the late afterglow.

Electrons released in metastable pooling reactions can have a kinetic energy of up to 7.4 eV, which is much greater that the electron temperature. Thus, pooling reactions can be an effective source of electron heating in the afterglow, producing ''superthermal'' electrons. Another source of superthermal electrons in the afterglow is superelastic collisions with metastables. The colliding electron can increase its energy by almost 11.6 eV. This latter mechanism is included in the fluid formulation of the electron energy balance as a contribution to the last term of Eq. (4).

In any gas discharge, the plasma potential with respect to the walls is established so that the flux of electrons to the wall is balanced by an equal flux of positive ions (assuming singly charged ions). For a Maxwellian EEDF the plasma potential is several times the electron temperature. However, when the EEDF contains a group of superthermal electrons, the plasma potential will rise to confine these electrons.[20] This may be the case in an afterglow argon plasma, depending on the rate I_0 at which superthermal electrons are produced. The ion flux to the walls is of the order of $\pi D_a n_0/L$ where n_0 is the plasma density at the center of the discharge, D_a is the ambipolar diffusion coefficient, and L is the interelectrode spacing. If the generation rate of superthermal electrons is small, $I_0 < D_a n_0$, these electrons do not affect the plasma potential which stays of the order of several kT_e/q. In the opposite case, $I_0 > D_a n_0$, the majority of the fast electrons must be trapped and the plasma potential can be as large as ϵ^*, the energy stored in a metastable atom. This is much larger than several kT_e/q, especially in the afterglow when kT_e/q drops below 1 eV. The conclusion is that, in the presence of a significant fraction of superthermal electrons, the plasma potential will decay slower compared to the case of no superthermal electrons.

Figure 4 shows the spatio-temporal dynamics of metastable density. It is worth mentioning that a pronounced minimum in the radial distribution of metastable density is

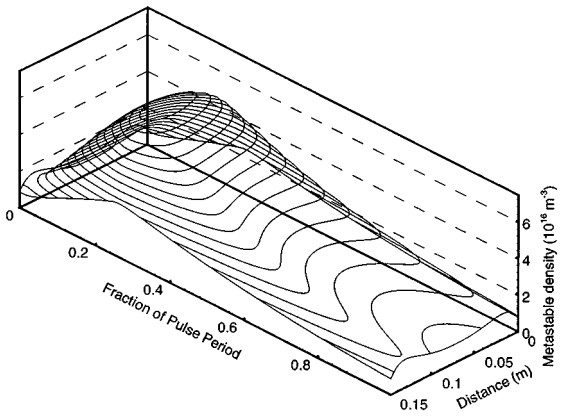

FIG. 4. Spatio-temporal dynamics of metastable density for a pulse period of 100 μs. No electrode bias.

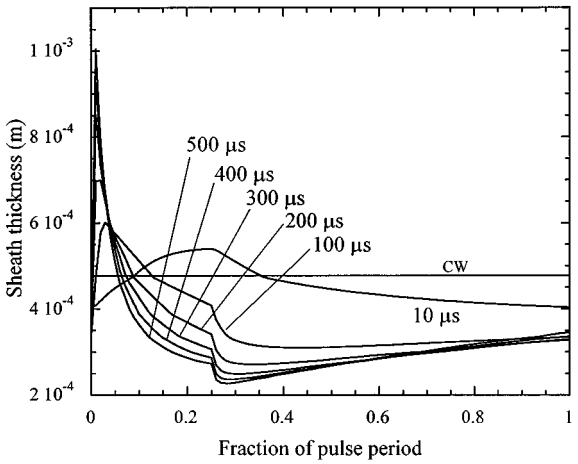

FIG. 6. Temporal evolution of the sheath thickness for different pulse periods. No electrode bias.

formed in the afterglow. This happens because no metastables are generated in the power-off fraction of the cycle (the excitation rate drops relatively rapidly) while the loss of metastables by superelastic collisions (see Table I) has a maximum at the center where the electron density has a maximum. This metastable profile also yields an on-axis minimum in the radial distribution of the metastable pooling reaction rate (not shown).

The spatio-temporal distribution of the electrostatic potential is shown in Fig. 5 for the pulse period of 100 μs. Rather rapid electron cooling in the afterglow results in a decrease of the plasma potential and a flattening of the potential distribution in the plasma. For a pulse period of 500 μs, the plasma potential at the end of the power-off fraction of the cycle drops down to 2.2 V.

The sheath thickness as a function of time is shown in Fig. 6. The plasma-sheath boundary was defined as the point where $(n_i-n_e)/n_i=0.1$. Interestingly enough, the time average sheath thickness decreases monotonically with increasing pulse period from 478 μm for cw to 317 μm for a 500 μs pulse period. For a given pulse period, the time evolution of the sheath thickness follows the time dependent variation of the Debye length; the latter increases with temperature and decreases with electron (ion) density. During the initial stages of the power-on fraction of the cycle (for times <0.05), the sheath increases in thickness because the electron temperature increases (longer Debye length) on a time scale short compared to the plasma density increase. Then, the sheath becomes thinner as the plasma density increases and the electron temperature drops (see Fig. 2). Right after power turn off (at time 0.25) the sheath thickness drops abruptly because of the electron temperature drop. At the later stages of the afterglow, the density effect on the Debye length dominates and the sheath thickness increases slowly as the plasma density drops slowly.

Figure 7 shows the time dependence of the ion energy flux (ion flux times ion energy) to the electrode for different pulse periods and for the same time-averaged power absorbed in the plasma (750 W/m^2). As expected, the amplitude of the ion energy flux modulation increases with increasing pulse period. However, the time-averaged ion energy flux has a minimum at a pulse period of about 200 μs

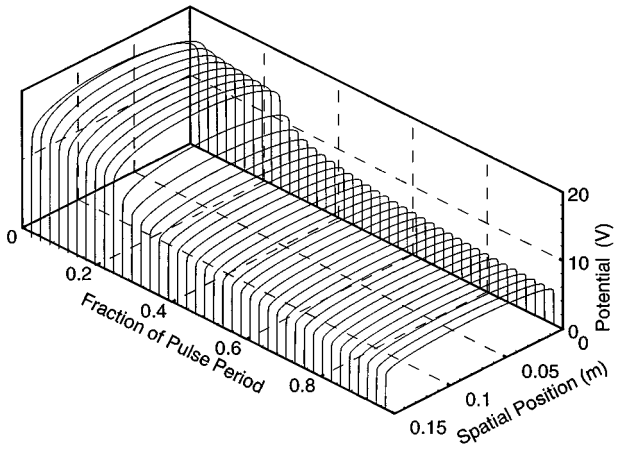

FIG. 5. Spatio-temporal variation of the electrostatic potential for a pulse period of 100 μs. No electrode bias.

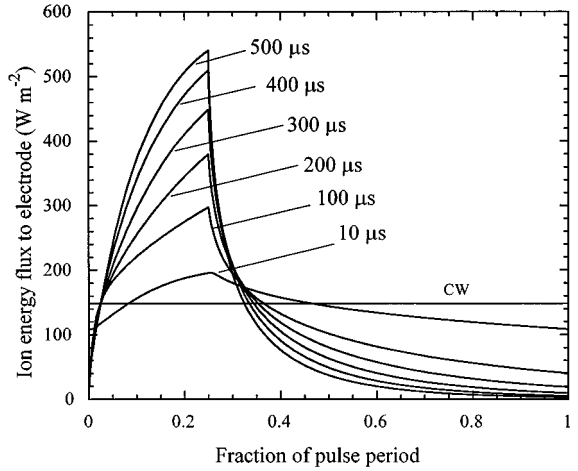

FIG. 7. Temporal evolution of the ion energy flux to the left electrode for different pulse periods. No electrode bias.

TABLE II. Time-averaged parameters of argon plasma for different pulse periods.

Pulse period (μs)	Electron density $\langle n_e\rangle_{\text{center}}$ (10^{17} m^{-3})	Electron temperature $\langle T_e\rangle_{\text{center}}$ (eV)	Ion energy flux $(P_{Ar^+})_{\text{elec.}}$ (Wm^{-2})	Time averaged sheath thickness (μm)
cw	1.02	2.50	148.08	477.6
10	1.11	2.34	143.19	453.3
100	1.39	1.82	127.13	363.3
200	1.48	1.62	125.27	337.5
300	1.51	1.50	127.51	325.1
400	1.50	1.41	131.90	319.9
500	1.49	1.33	132.63	316.6

(see also Table II). This suggests the existence of an optimal pulse period to achieve minimum wafer heating for a given power into the plasma.

Simulation results are summarized in Table II where several time-averaged plasma parameters are shown for different pulse periods. It is seen that the time-averaged electron temperature decreases with an increase of the pulse period. The ion energy flux has a minimum for a pulse period of about 200 μs.

B. The effect of rf bias

Before applying a bias, the discharge was first allowed to relax to a periodic steady state. The rf bias was applied at a dimensionless time 0.3, i.e., shortly after the plasma heating power was turned off. Application of an rf bias results in modification of the rf sheaths near the walls and in changes of the plasma potential and particle fluxes to the plasma boundaries. The bias frequency is a parameter of considerable interest in etching technology. In general, the impedance of a rf sheath may be capacitive or resistive depending on the ratio of the ion transit time across the sheath, τ, and the applied field frequency, ω.[22,23,36] For $\omega<\omega_i(n_s)$ where ω_i is the ion plasma frequency and n_s is the plasma density at the plasma-sheath boundary, the displacement current in the sheath is low compared to the conduction current. For resistive sheaths $\tau\approx 1/\omega_i(n_s)$.[23] Moreover, at $\omega\tau<1$ ions cross the sheath in a short time compared to the period of the bias voltage, and are accelerated by the instantaneous sheath field. In the opposite case, $\omega\tau>1$, ions cross the sheath slowly compared to the period of the bias voltage, and are accelerated by the time-averaged sheath field. In low pressure high density plasmas, the sheath is rather thin (see Fig. 7), so that $\omega\tau\approx 1$ at $\omega/2\pi\approx 10$ MHz. Thus, for the bias frequencies of interest, $\omega\tau<1$, and the sheath has a major resistive component. In the intermediate frequency regime ($\omega\tau\approx 1$), phase shifts between ion velocity, ion density, and sheath potential can produce interesting effects, some of which are discussed below.

As described in Refs. 22 and 23, the plasma potential $V_p(t)$ is harmonic in a system with purely capacitive rf sheaths, whereas it is far from harmonic in a system with resistive sheaths. Because of the high electron mobility, the plasma potential can't be negative with respect to any surface in contact with the plasma. When the potential of a driven electrode decreases, electrons escape quickly leaving behind a net positive charge which prevents further decrease of plasma potential and traps the remaining electrons.[37] The plasma potential ''rides'' above the potential of the biased electrode when the latter is positive with respect to ground and has a value of a few kT_e/q above ground when the bias potential is negative. The amplitude of oscillation of $V_p(t)$ depends on the effective areas of the grounded surface and the excitation electrode that are in contact with the plasma. This behavior is born out in Fig. 8 which shows the time variations of the plasma potential at the discharge center when a 100 kHz bias voltage (40 V peak to peak) is applied on the left electrode, in the afterglow, during dimensionless times 0.3–0.7. The plasma potential is not ''sinusoidallike'' (it is clipped), implying a resistive sheath.

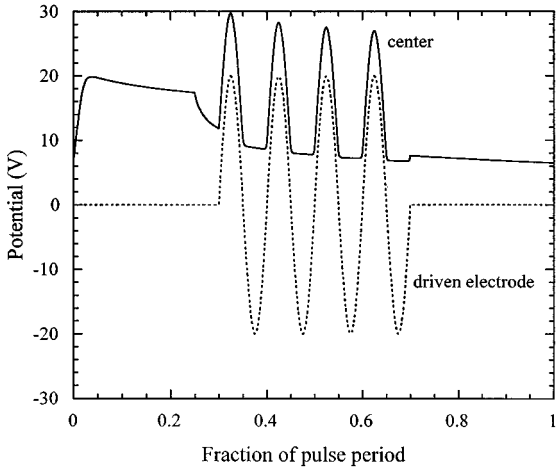

FIG. 8. Plasma potential in a discharge pulsed with a period of 100 μs. A 40 V peak-to-peak bias with a frequency of 100 kHz is applied during dimensionless times 0.3–0.7.

Resistive sheath behavior was observed in our simulations for a wide range of frequencies, namely 100 kHz–10 MHz. At these frequencies, electrons respond to the instantaneous rf field (Fig. 9). The electron flux diminishes to zero during the negative swings of the applied bias. The ion response depends on bias frequency. The amplitude of the ion flux oscillations is expected to have a maximum at $\omega\tau\approx 1$, i.e., the amplitude increases with ω up to 10 MHz for our discharge conditions (Fig. 10). At low frequencies (i.e., 100 kHz), the ion flux at the electrode is only weakly modulated. This can be understood by neglecting the time derivative in Eq. (1) (quasistatic approximation) and also dropping the reaction term. The result is an approximately spatially invariant flux throughout the sheath. In this approximation, the ion velocity at the electrode is almost in step with the oscillations of the sheath potential (Fig. 11). The ion density at the electrode is out of phase with respect to the ion velocity (not shown). With increasing ω, the time delay of $n_i(t)$ becomes notable; the time derivative in Eq. (1) can't be dropped. This results in an increase of the amplitude of ion flux $\Gamma_i(t)$ oscillations shown in Fig. 10.

At present, no simple sheath model is available to de-

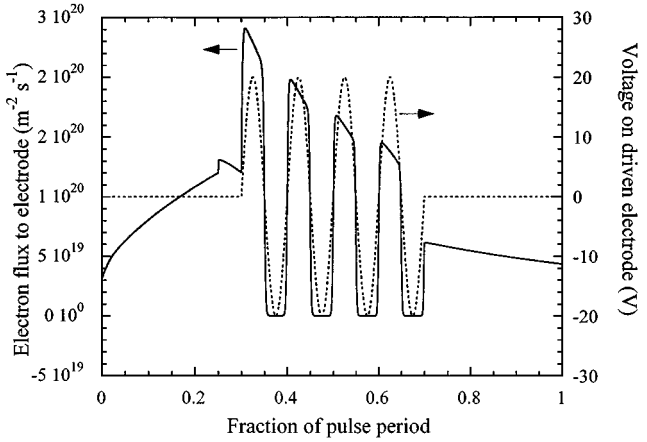

FIG. 9. Electron flux to the driven (left) electrode in the afterglow of a discharge pulsed with a period of 100 μs. A 40 V peak-to-peak bias with a frequency of 100 KHz is applied during dimensionless time 0.3–0.7.

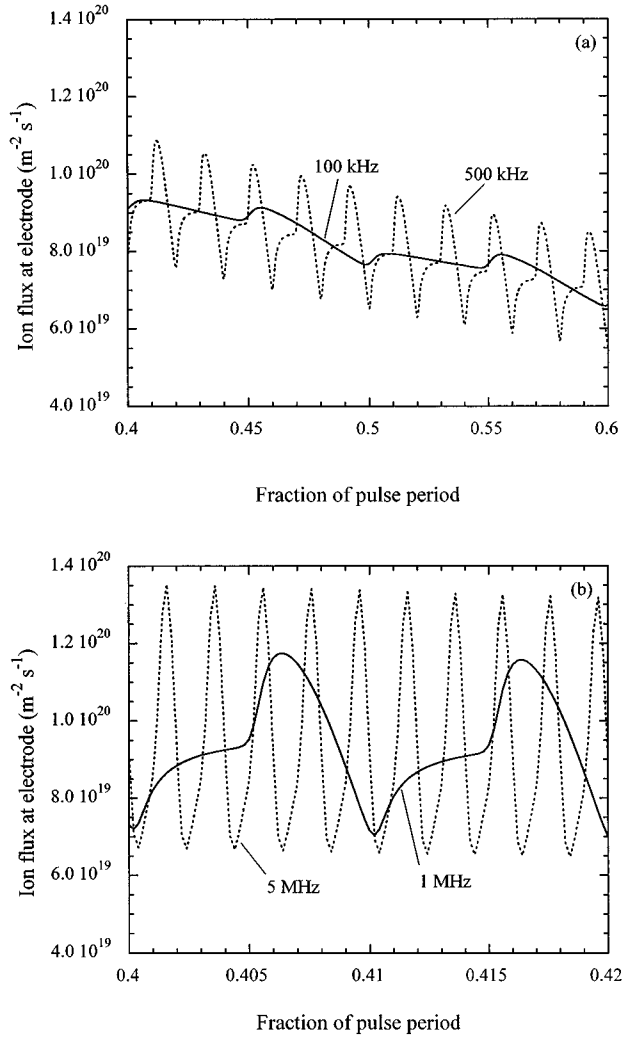

FIG. 10. Ion flux to the driven (left) electrode in the afterglow of a discharge pulsed with a period of 100 μs. A 40 V peak-to-peak bias is applied during dimensionless times 0.3–0.7 with different frequencies: (a) 100 and 500 kHz bias frequency; only the time window 0.4–0.6 is shown, (b) 1 and 5 MHz frequency; only the time window 0.4–0.42 is shown.

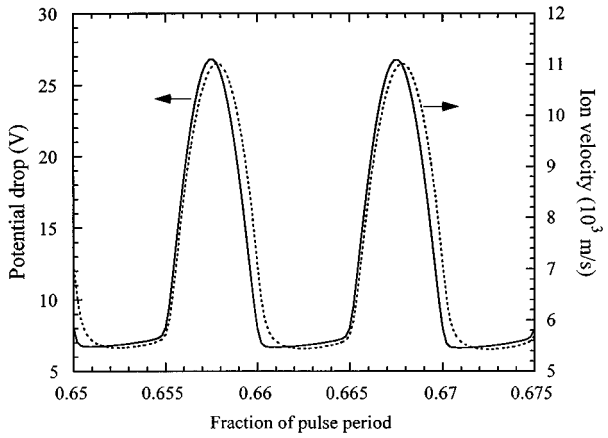

FIG. 11. Sheath potential drop and ion velocity of ions bombarding the driven electrode in the afterglow of a discharge pulsed with a period of 100 μs. A 40 V peak-to-peak bias with a frequency of 1 MHz is applied during dimensionless times 0.3–0.7. Note that only the time window 0.6–0.675 is shown in this figure.

scribe the sheath behavior observed in our simulations. The Riley model[38] which accounts for ion transit-time effects at intermediate frequencies ($\omega\tau \approx 1$), assumes a constant ion flux in the sheath, essentially neglecting the time derivative term in the ion density equation [Eq. (1)]. Our simulations indicate that the $\partial n_i/\partial t$ term is important in Eq. (1) for describing the sheath dynamics in rf-biased high density plasmas. An enhancement of the Riley model is under way[39] which includes this time derivative.

C. Limitations of fluid approach

The limitations of fluid models regarding treatment of electrons have been discussed in a number of publications (see, for example, Refs. 36 and 40). Up to date, kinetic treatment of electrons in ICPs has been performed mainly for steady-state collisional plasmas.[41,42] It was found that, at least in rare gases, the EEDF is Maxwellian in the elastic energy range due to Coulomb interactions among electrons.[43] Also, the kinetics of trapped and free electrons was shown to be entirely different.[44] We expect several new kinetic effects to be important in pulsed plasmas, which can't be captured by a fluid model. First, creation of fast (superthermal) electrons by metastable reactions may result in high energy peaks in the EEDF, or formation of a wide ''tail,'' depending on discharge conditions.[20] Second, the velocity distribution of free electrons can be notably anisotropic in a weakly collisional plasma.[44,45] This happens because only electrons in the loss cone are capable of escaping the discharge. In the planar case considered here, the axial kinetic energy of electrons at the center $mu_x^2/2$ must exceed the plasma potential qV_p with respect to the wall for these electrons to escape. Thus, one could expect the formation of a tail of electrons with large $u_y^2+u_z^2$ in a weakly collisional afterglow plasma when $V_p(t)$ decreases with time. These electrons can get into the loss cone and escape only as a result of collisions which are relatively rare. Finally, anisotropic electron velocity distributions must also appear at the biased electrode that extracts charged species out of the plasma.

In this work, we have used the cold plasma approximation to calculate the rf field profile and power absorption in the plasma. This is another place where kinetic treatment of electrons can provide more accurate results. In weakly collisional plasmas, the thermal motion of electrons results in the anomalous penetration of electromagnetic fields into the plasma[29] and the appearance of non-Joule electron heating.[44] These effects could modify the plasma dynamics in the power-off phase of the discharge.

IV. SUMMARY

We have developed a one-dimensional fluid model of pulsed-power inductively coupled plasmas and have used this model to investigate the spatio-temporal dynamics of an argon plasma at 10 mTorr. The one-dimensional formulation allowed both plasma and sheath to be treated self-consistently within the same framework. The sheath thickness was a complicated function of time in the pulsed plasma. Two-step ionization was negligible during the active discharge, but became the dominant mechanism of electron production in the afterglow. Generation of superthermal electrons by metastable reactions can have an impact on the time scale of the plasma potential decay in the afterglow. Particular attention was paid to extraction and acceleration of positive ions by a rf bias applied in the afterglow stage of the pulsed discharge. For the entire range of practical bias frequencies the sheath is resistive in nature. Significant oscillations of the ion flux at the driven electrode were observed and are related to ion transit-time effects at $\omega\tau \approx 1$. For a constant time-average power, the time-average ion energy flux bombarding the wafer has a minimum with respect to the pulse period. This has implications for the wafer thermal budget.

ACKNOWLEDGMENT

Work at the University of Houston was supported by the National Science Foundation Grant Nos. CTS-9216023 and CTS-9713262.

[1]H. Sugai, K. Nakamura, Y. Hikosaka, and M. Nakamura, J. Vac. Sci. Technol. A **13**, 887 (1995).
[2]P. Jiang, D. J. Economou, and C. B. Shin, Plasma Chem. Plasma Process. **15**, 383 (1995).
[3]L. Overzet, J. Verdeyen, R. Roth, and Carasco, Mater. Res. Soc. Symp. Proc. **98**, 321 (1987).
[4]R. Boswell and R. Porteous, J. Appl. Phys. **62**, 3123 (1987).
[5]S.-K. Park and D. J. Economou, J. Electrochem. Soc. **138**, 1499 (1991).
[6]J. Verdeyen, J. Bederman, and L. Overzet, J. Vac. Sci. Technol. A **8**, 1851 (1990).
[7]A. Howling, L. Sansonnens, J.-L. D. , and Ch. Hollenstein, J. Appl. Phys. **75**, 1340 (1994).
[8]S.-K. Park and D. J. Economou, J. Electrochem. Soc. **137**, 2103 (1990).
[9]S. Samukawa and T. Mieno, Plasma Sources Sci. Technol. **5**, 132 (1996).
[10]T. H. Ahn, K. Nakamura, and H. Sugai, Plasma Sources Sci. Technol. **5**, 139 (1996).
[11]T. Shibayama, H. Shindo, and Y. Horiike, Plasma Sources Sci. Technol. **5**, 254 (1996).
[12]J. C. Arnold and H. H. Sawin, J. Appl. Phys. **70**, 5314 (1991).
[13]T. Kinoshita, M. Hane, and J. McVittie, J. Vac. Sci. Technol. B **14**, 560 (1996).
[14]G. S. Hwang and K. P. Giapis, J. Vac. Sci. Technol. B **15**, 70 (1997).
[15]S. Samukawa, H. Ohtake, and T. Mieno, J. Vac. Sci. Technol. A **14**, 3049 (1996).
[16]S. Ashida, M. R. Shim, and M. A. Lieberman, J. Vac. Sci. Technol. A **14**, 391 (1996).
[17]M. Meyyappan, Jpn. J. Appl. Phys., Part 1 **36**, 4820 (1997).
[18]J. D. Bukowski, R. A. Stewart, D. B. Graves, and P. Vitello, in *Proceedings of the 1st International Symposium on Process Control, Diagnostics and Modeling in Semiconductor Manufacturing*, edited by M. Meyyappan, D. J. Economou, and S. W. Butler (Electrochemical Society, 1995), Vol. 95, p. 564.
[19]L. J. Overzet, Y. Lin, and L. Luo, J. Appl. Phys. **72**, 5579 (1992).
[20]N. B. Kolokolov, A. A. Kudryavtsev, and A. B. Blagoev, Phys. Scr. **50**, 371 (1994).
[21]S. A. Gutsev, A. A. Kudryavtsev, and V. A. Romanenko, Tech. Phys. **40**, 1131 (1995).
[22]K. Kohler, D. E. Horne, and J. W. Coburn, J. Appl. Phys. **58**, 3351 (1985).
[23]A. M. Pointu, J. Appl. Phys. **12**, 4113 (1986).
[24]M. S. Barnes, J. C. Foster, and J. H. Keller, IEEE Trans. Plasma Sci. **19**, 240 (1991).
[25]V. E. Golant, A. P. Zhilinsky, I. E. Sakharov, and S. C. Brown, *Fundamentals of Plasma Physics* (Wiley, New York, 1980).
[26]D. P. Lymberopoulos and D. J. Economou, J. Res. Natl. Inst. Stand. Technol. **100**, 473 (1995).
[27]D. P. Lymberopoulos and D. J. Economou, J. Appl. Phys. **73**, 3668 (1993).
[28]R. H. Cohen and T. D. Rognlien, Plasma Sources Sci. Technol. **5**, 442 (1996).
[29]V. I. Kolobov and D. J. Economou, Plasma Sources Sci. Technol. **6**, 1 (1997).
[30]V. A. Godyak, R. B. Piejak, and B. M. Alexandrovich, Plasma Sources Sci. Technol. **3**, 169 (1994).
[31]M. M. Turner, Phys. Rev. Lett. **71**, 1844 (1993).
[32]V. Vahedi, M. A. Lieberman, G. DiPeso, T. D. Rognlien, and D. Hewett, J. Appl. Phys. **78**, 1446 (1995).
[33]T. Hughes, *The Finite Element Method* (Prentice–Hall, Englewood Cliffs, NJ, 1987).
[34]A. C. Hindmarsh, in *Scientific Computing*, edited by R. S. Stepleman (IMACS, 1983), p. 55.
[35]R. Wise, D. P. Lymberopoulos, and D. J. Economou, Appl. Phys. Lett. **68**, 2499 (1996).
[36]T. E. Nitschke and D. B. Graves, IEEE Trans. Plasma Sci. **23**, 717 (1995).
[37]R. H. Bruce, J. Appl. Phys. **52**, 7064 (1981).
[38]P. Miller and M. E. Riley, J. Appl. Phys. **82**, 3689 (1997).
[39]M. Riley (personal communication).
[40]V. I. Kolobov and V. A. Godyak, IEEE Trans. Plasma Sci. **23**, 603 (1995).
[41]V. I. Kolobov and W. N. G. Hitchon, Phys. Rev. E **52**, 972 (1995).
[42]U. Kortshagen, I. Pukropski, and L. D. Tsendin, Phys. Rev. E **51**, 6063 (1995).
[43]V. I. Kolobov, G. J. Parker, and W. N. G. Hitchon, Phys. Rev. E **53**, 1110 (1996).
[44]V. I. Kolobov, D. P. Lymberopoulos, and D. J. Economou, Phys. Rev. E **55**, 3408 (1997).
[45]U. Kortschagen, G. J. Parker, and J. E. Lawler, Phys. Rev. E **54**, 6746 (1996).